Journal of Applied Mechanics and Technical Physics, Vol. 46, No. 1, pp. 141–147, 2005

NUMERICAL SIMULATION OF PLASTIC-FLOW LOCALIZATION FOR SIMPLE SHEAR

V. M. El'kin, V. N. Mikhailov, T. Yu. Mikhailova

UDC 01-201; 01-315

An algorithm was developed to numerically simulate plastic-flow localization for simple shear of a thermally plastic and viscoplastic material. The algorithm is based on solving the partial differential equations describing continuum flow. The closing equation is the constitutive relation known in the literature as the power law linking the plastic-strain rate to the flow stress, temperature, and accumulated plastic strain. Calculated relations for the time evolution of the shear-band width and the temperature and plastic strains localized in it agree satisfactorily with experimental relations. Good agreement with experimental results is also obtained for the sample temperature distribution at the developed stage of the localization process.

Key words: *plastic-flow localization, simple shear, numerical simulation.*

Introduction. At present, numerous experimental studies have shown that in high-velocity deformation of solids (metals, rocks, or polymers), initially homogeneous plastic deformation becomes inhomogeneous. The inhomogeneity of the deformation process is manifested, in particular, in the formation of so-called adiabatic shear bands observed in metallographic studies of samples subjected to dynamic loading. The mechanism of formation of these bands proposed by Zener and Hollomon [1], which has already become classical, reduces to the following. Plastic shear occurs initially in several weak zones with heat release due to the work of plastic deformation, which, under dynamic loading conditions, has no time to encompass the entire volume of the sample. Local reduction in the yield strength in the heated zone results in plastic-flow activation in this zone and, hence, in even higher heat release and further reduction in the yield strength. The process thus develops disastrously up to failure of the material in the shear band and, in some cases, up to melting of the failure surface. Subsequent fast cooling leads to a change in the material microstructure in the shear band, as was observed in metallographic studies of samples after loading.

Formulation of the Problem. The problem of simple shear deformation of an infinite layer of an isotropic viscoplastic material of thickness $2d$ can be formulated as follows (see, for example, [2, 3]). The lower and upper boundaries of the layer move oppositely at a velocity V_0 in a certain chosen direction. Because of the symmetry of the problem, the midplane of the layer has a velocity equal to zero, which makes it possible to formulate the problem for only half of the layer with the lower boundary fixed and the upper boundary moving at a constant velocity V_0 in the y direction (Fig. 1). In this one-dimensional formulation, the coordinates and temperature of a mass point are written as

$$y = y_0 + U(x,t), \qquad x = x_0, \qquad z = z_0, \qquad T = T(x,t),$$

where x, y, and z are the current coordinates, x_0, y_0, and z_0 are the initial coordinates of the point, U is the displacement in the y direction, T is the temperature, and t is time. The Oy and Oz axes lie in the plane of the lower boundary of the layer, and the Ox axis is normal to this plane.

Zababakhin Institute of Technical Physics, Snezhinsk 456770; mikhailov@gdd.ch70.chel.su. Translated from Prikladnaya Mekhanika i Tekhnicheskaya Fizika, Vol. 46, No. 1, pp. 173–180, January–February, 2005. Original article submitted January 19, 2004.

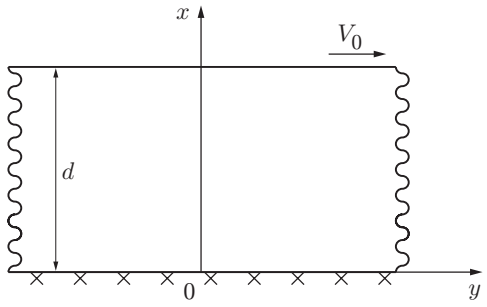

Fig. 1. Diagram of simple shear.

The equations of motion and heat conduction in this (Cartesian) coordinate system are written as

$$\rho_0 \dot{V} = \frac{\partial \sigma}{\partial x}, \qquad \rho_0 c \dot{T} = \lambda \frac{\partial^2 T}{\partial x^2} + \gamma \sigma \dot{\varepsilon}_p, \tag{1}$$

where ρ_0, c, and λ are the density, heat capacity, and thermal conductivity of the layer material, respectively, σ is the flow stress, $V = \dot{U}$ is the velocity of the mass point, ε_p is the plastic strain, γ is the fraction of the work of plastic deformation converted to heat. Here and below, the dot above the variable denotes differentiation with respect to time.

The initial and boundary conditions for the velocity and displacement are determined by the loading model given above:

$$\begin{gathered} U(x,0) = 0, \qquad V(x,0) = V_0 x/d, \\ U(0,t) = 0, \quad V(0,t) = 0, \qquad U(d,t) = V_0 t, \quad V(d,t) = V_0. \end{gathered} \tag{2}$$

The boundary conditions on the temperature define the adiabaticity of process:

$$\frac{\partial T}{\partial x}(0,t) = \frac{\partial T}{\partial x}(d,t) = 0; \tag{3}$$

the initial conditions corresponds to a uniform temperature distribution:

$$T(x,0) = T_0. \tag{4}$$

It is assumed that the total strain is the sum of the elastic strain ε_e and the plastic strain ε_p:

$$\varepsilon \equiv \frac{\partial U}{\partial x} = \varepsilon_e + \varepsilon_p. \tag{5}$$

Hence,

$$\dot{\sigma} = G\Big(\frac{\partial V}{\partial x} - \dot{\varepsilon}_p\Big), \tag{6}$$

where G is the shear modulus.

The constitutive equation for the viscoplastic layer material is written as the simple power-law model

$$\sigma = \sigma_0 \Big(\frac{\dot{\varepsilon}_p}{\dot{\varepsilon}_*}\Big)^m \Big(\frac{\varepsilon_p}{\varepsilon_*}\Big)^n \Big(\frac{T}{T_*}\Big)^{-\nu}. \tag{7}$$

Here m, n, and ν are factors that describe the sensitivity of the material to the loading rate, deformation strengthening, and thermal softening, respectively, σ_0 is the flow stress for $\dot{\varepsilon}_p = \dot{\varepsilon}_*$ and $\varepsilon_p = \varepsilon_*$, and $T = T_*$.

Numerical Simulation. Equations (1)–(7) are solved numerically on the segment $[0, d]$ using a uniform spatial grid:

$$x_i = i\Delta x, \qquad i = 0, \ldots, N, \quad x_N = d.$$

The space derivatives on the grid are calculated using spline functions. The use of splines for function interpolation, numerical differentiation, and integration is described in numerous papers (see, for example, [7]).

For a function $y = f(x)$ with values specified as grid nodes $y_i = f(x_i)$, the interpolation cubical spline is written as

$$S(x) = y_i + C_{1,i}(x - x_i) + C_{2,i}(x - x_i)^2 + C_{3,i}(x - x_i)^3,$$

where $C_{1,i}$, $C_{2,i}$, and $C_{3,i}$ are coefficients to be determined.

The step in time Δt is determined from the Courant condition of solution stability:

$$\dot{\varepsilon}\Delta t \leqslant \Delta x \min\left[1/C_s, \Delta x/(2r)\right]. \tag{8}$$

Here $r = \lambda/(\rho_0 c)$ and $C_s = (G/\rho_0)^{1/2}$ is the velocity of the elastic shear wave. Condition (8) is a combination of the stability conditions for the equations of motion and heat conduction.

Let us note some features that arise in the simulation of experiments with Kolsky bars using system (1)–(7). In these experiments, the strain rate is $\dot{\varepsilon}_0 \approx 10^2$–$10^4$ sec^{-1} and the sample size is $2d = 2.5$ mm. In this case, satisfaction of the stability condition for the equation of motion leads to an extremely small step in time. For the parameters G and ρ_0 typical for steel and for $\Delta x = 0.01d$ (100 intervals), the step in time is $\dot{\varepsilon}\Delta t \leqslant 10^{-11}$ and the computation time for one version becomes unrealistically large. However, in this case, the ratio of the sound velocity to the velocity of motion of the medium is also large:

$$C_s/V = G/(\rho_0 V) \approx 10^{19};$$

i.e., at each time, a homogeneous state of stress ($\partial\sigma/\partial x = 0$) occurs in the material. Thus, from this point of view, this type of tests is quasistatic and the calculations in this case can be performed eliminating the equation of motion (1) from system (1)–(7). Integrating Eq. (7) over x and t, we obtain the following expression for the stress:

$$\sigma(t) = G\Big(\int\limits_0^1 \varepsilon\, dx - \int\limits_0^1 \varepsilon_p\, dx\Big) = G\Big(t - \int\limits_0^1 \varepsilon_p\, dx\Big).$$

The function $\varepsilon_p(x)$ is integrated using the corresponding spline.

In this case, the stability of the solution of the system is described by the Courant condition for the heat-conduction equation

$$\dot{\varepsilon}\Delta t \leqslant \Delta x^2/(2r) \approx 10^{-3}.$$

With this step in time, the computation time for one version becomes quite reasonable.

System (1)–(7) is implemented in the SHEAR BAND numerical code in Pascal using the Delphi integrated development environment.

The simulation of shear band formation and development for simple shear was considered in [2, 3], where the effect of material parameters on the nature of localization was in qualitative agreement with experimental observations. In [3] a simple comparative criterion of localization is formulated on the basis of simulation results. Numerical simulation has been widely used to study the behavior of shear bands. The results, as a rule, have been qualitatively compared with experimental data. However, it is of great interest to directly compare computation and experimental data. In the present study, the results of numerical simulations of shear band development are directly compared with the experimental data of [4, 5]. In the cited papers, shear band formation was studied in detail for dynamic torsion of tubular samples of low-doped steels (HY-100, 1080 CRS, and 1020 HRS) using a Kolsky torsional setup. In these experiment, the strain rate was $(1\text{–}5) \cdot 10^3$ sec^{-1}; therefore, the calculations were conducted in a quasistatic approximation.

For numerical simulation of shear band formation, it is necessary to specify the initial inhomogeneity that initiates the development of plastic flow instability. In the experiments of [4, 5], this inhomogeneity was not specified but, as is noted in [4], on the axis of the tubular samples there was a 5–10% difference in thickness apparently due the sample production process. In the calculations, this inhomogeneity of the sample was modeled by local weakening of the strength parameter σ_0 in the form

$$\sigma_0(x) = \sigma_{00}[1 - \delta\cos(\pi x/(2h)],$$

where δ is the perturbation amplitude and h is the width of the perturbation zone. Preliminary calculations showed that the parameters δ and h have a significant effect on the development of the localization process, and the fact that the difference in sample thickness was not measured in the experiments considerably hindered the comparison

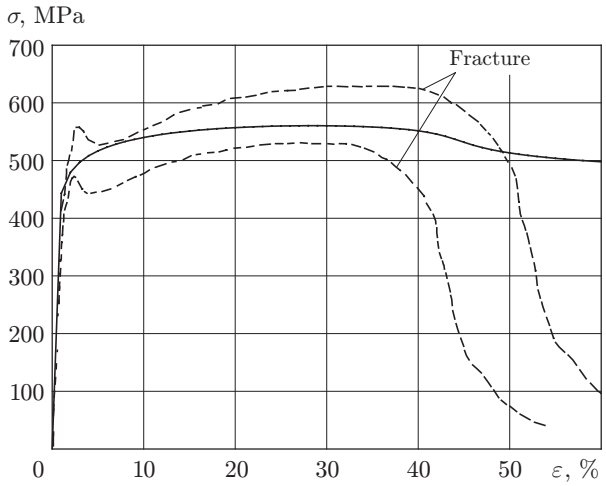

Fig. 2. Experimental and calculated loading diagrams for HY-100 steel at standard temperature and a strain rate of 1600 $\sec^{-1}$: the dashed curves are the boundaries of the spread zone of the experimental data of [4]; the solid curve is the calculation.

TABLE 1

Steel grade	ν	n	m	σ_{00}, MPa	δ
HY-100	0.33	0.08 (0.107)	0.0117	463 (510)	0.1
1018 CRS	0.38	0.015	0.019	486 (436)	0.022
1020 HRS	0.51	0.12	0.0133	296 (261)	0.015

of the simulation results and experimental data. In all calculations of the present study, the perturbation zone had a width $h = d$ and the value of the perturbation amplitude was chosen so as to obtain a fit between the calculated and experimental strains $\varepsilon_{\sigma\max}$ that provide a maximum on the σ–ε (stress–strain) diagram. We note that the spread in $\varepsilon_{\sigma\max}$ from experiment to experiment is rather great (approximately 50%), which is apparently due to oscillations of the uncontrolled difference in the sample thickness.

Calculation Results and Comparison of with Experiment. The mathematical modeling of the experiments of [4, 5] is considerably simplified by the fact that the parameters of the constitutive equations (7) for the tested steels were chosen from the results of preliminary experiments. We note, however, that the plastic strain rate, plastic strain, and temperature in the shear band are far beyond the boundaries of the regions in which these parameters were determined. Therefore, a certain correction of these parameters is quite permissible. Such a correction was made for the deformation strengthening parameter n and the strength parameter σ_{00}. The goal of this correction was to achieve that the calculated σ–ε diagram was in the range of experimental values.

Figure 2 gives the calculation results and their comparison with experimental data (for HY-100 steel) with allowance for the spread. Although the calculated curve is in the zone of spread of the experimental results, the curves differ in nature. In particular, the region of strengthening of the experimental curves has a larger duration. As a result, the initial stage of localization of plastic deformation recorded in the experiment is in the immediate proximity to the stress maximum, whereas in the calculation notable inhomogeneity occurs much earlier. In addition, the stress drop (after attainment of the maximum) on the experimental curves is faster than that on the calculated curve (the segment of sharp flow stress drop corresponds to failure of the sample, and in this case, a comparison with the calculated curve is meaningless). In this connection, it should be recognized that the constitutive relation in the power-law form proposed in [4, 5] does not provide the best description of the experimental loading diagram of HY-100 steel, even ignoring the yield spike. Nevertheless, this constitutive equation was used in the calculations.

Table 1 gives the values used in the calculations of the parameters of the constitutive relation (7), which primarily coincide with the experimental values of [4, 5]. For the parameters corrected during the solution, their experimental values are given in parentheses. In addition, for all steels the following parameters were used: $\gamma = 1$, $d = 1.25$ mm, $\lambda = 54$ W/(m·K), $\rho_0 = 7900$ kg/m^3, $c = 500$ J/(kg·K), and $G = 81$ GPa.

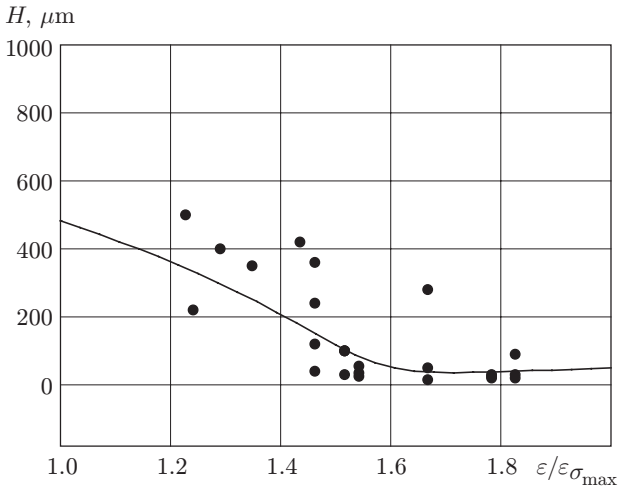

Fig. 3

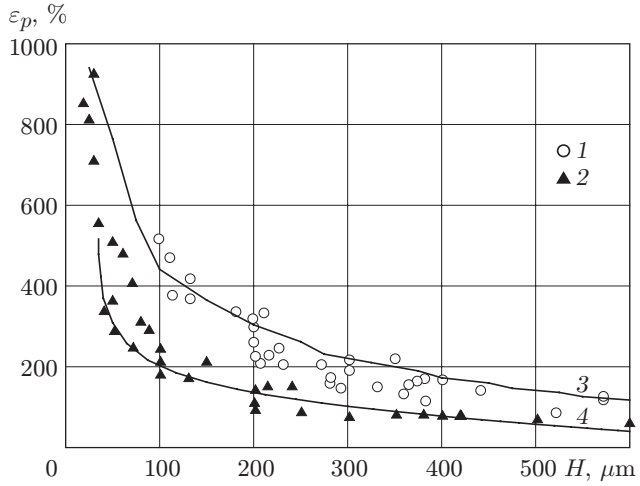

Fig. 4

Fig. 3. Shear bandwidth versus average normalized strain for HY-100 steel: the points refer to the experiment of [4] and the curve refers to the calculation.

Fig. 4. Average strain in the shear band versus bandwidth: experimental values of [4] for 1018 CRS steel (1) and HY-100 steel (2); calculations for 1018 CRS steel (3) and HY-100 steel (4).

In [4], the widths of the shear and strain bands in this zone were measured for HY-100 steel. The width of the shear band was determined as the length of the segment on the sample axis that corresponded to the constant slope of the grid line applied using lithography on the sample surface before loading. However, the permissible degree of deviation from this slope is not given. Therefore, in the calculations, as the shear bandwidth we used the width of the region in which the plastic strain exceeded 70% of the maximum value (by analogy with the determination of the pulse width in electrical engineering). Thus, the methods used to determine the shear bandwidth H in the experiment and calculations, generally speaking, were different. Therefore, initially, we attempted to find a correlation between them. However, unexpectedly, it turned out that the calculated and experimental data were in satisfactory agreement (Fig. 3). In Fig. 3, the abscissa is the nominal strain averaged over the sample and normalized by the strain at which the flow stress becomes maximum. The introduction of this variable is explained as follows. According to the existing concepts of the localization onset, supported by experimental data [4, 5], the point of reference of shear band formation is the strain at which the flow stress reaches the maximum. However, the spread in the values of $\varepsilon_{\sigma\,\max}$ in the experiments is large enough, and, hence, it seems reasonable to use the normalized strain.

Figure 4 shows a comparison of experimental and calculated dependences of the average strain in the shear band versus bandwidth for HY-100 and 1018 CRS steels. It is evident that the calculated and experimental data agree well for shear bandwidth from 30 to 600 μm. The very large experimental strains in the shear band $\varepsilon > 600\%$ for HY-100 steel correspond to the third stage of development of the localization process, which is characterized by considerable inhomogeneity of the deformation on the circumference of the sample. In addition, at this stage, the shear band does not lie in one cross-sectional plane of the sample. Thus, the development of the shear band becomes considerably non-one-dimensional and cannot be modeled using a one-dimensional program.

In [4], the temperature variation in time was measured by recording the infrared radiation from the sample surface at twelve points along its axis. Unfortunately, the three-dimensional plots "time–transducer number–transducer signal" presented there cannot be used for comparison with the calculated temperature variation in time at different points on the sample axis. For comparison, data on the temperature distribution on the axis were used. At the moment of failure, the average strain of the sample $\varepsilon_{\max}$, like the strain $\varepsilon_{\sigma\,\max}$, has a considerable spread and there is an obvious correlation between them. Because of this correlation, the spread in the normalized quantity $\varepsilon_{\max}/\varepsilon_{\sigma\,\max}$ is much smaller and is in the range 1.8–2.0. The temperature distribution was calculated for these extreme values of the maximum strain. Since the temperature measured in the experiment is the average over the

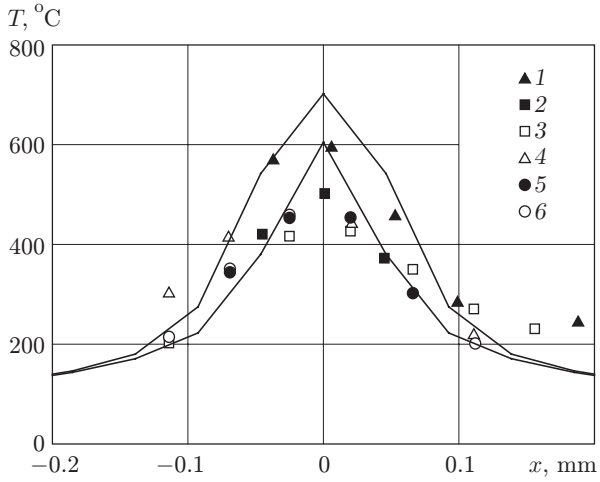

Fig. 5. Temperature distribution on the sample axis in the neighborhood of the shear band: solid curves refer to calculations; points 1–6 correspond to experimental data from [5].

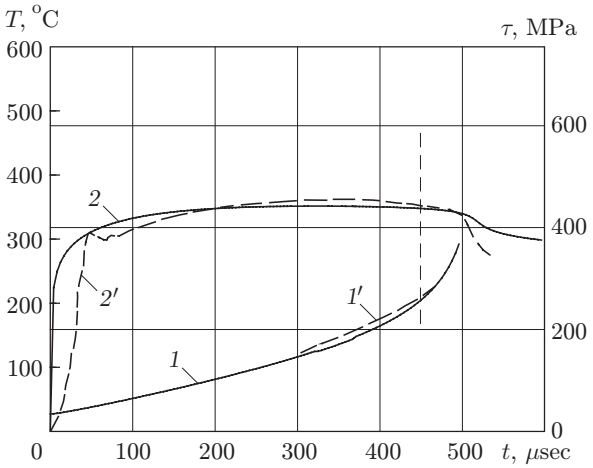

Fig. 6

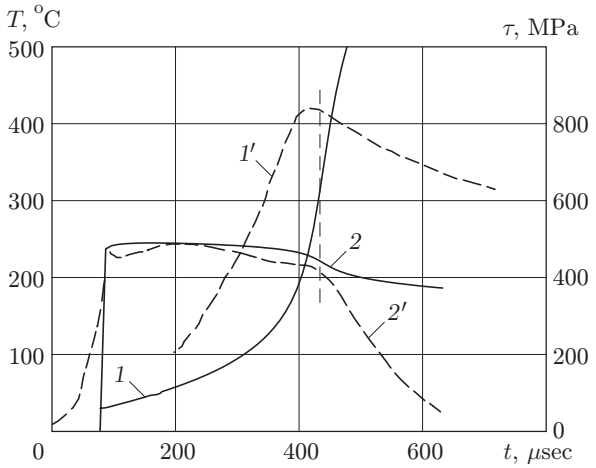

Fig. 7

Fig. 6. Temperature (curves 1 and 1′) and stress (curves 2 and 2′) versus time for 1020 HRS steel ($\dot{\varepsilon}_0 = 2400$ sec^{-1}): the dashed curves refer to the experiment of [5] and the solid curves refer to calculations; the vertical dashed line shows the moment of failure of the sample.

Fig. 7. Temperature (curves 1 and 1′) and stress (curves 2 and 2′) versus time for 1018 CRS steel ($\dot{\varepsilon}_0 = 1100$ sec^{-1}): the dashed curves refer to the experiment of [5] and the solid curves refer to calculations; the vertical dashed line shows the moment of failure of the sample.

size of the spot (35 μm) whose infrared radiation is recorded, the calculated results were averaged in an appropriate way for comparison with experiment. Figure 5 gives a comparison of the calculated and experimental data. From the plots given above, it is evident that the calculation data for the two extreme values of the maximum strain are in good agreement with the experimental results.

Figures 6 and 7 give experimental and calculated loading diagrams in time for 1020 HRS and 1018 CRS steels [5] and the time dependence of the temperature in the center of the shear band. It is evident that for 1020 HRS

steel, good agreement between the experimental and calculated data is obtained, whereas for 1018 CRS steel, the agreement is primarily qualitative.

Thus, although the employed constitutive equation is simple and (as noted above) is not quite adequate to experimental data, the numerical simulation provides a satisfactory fit to the experimental results on dynamic torsion of samples of HY-100, 1018 CRS, and 1020 HRS steels.

REFERENCES

1. C. Zener and J. H. Hollomon, "Effect of strain rate on plastic flow of steel," *J. Appl. Phys.*, **15**, 22–32 (1944).
2. T. G. Shawki and R. J. Clifton, "Shear band formation in thermal viscoplastic materials," *Mech. Mater.*, No. 8, 13–43 (1987).
3. V. M. El'kin, "Localization of plastic flow in simple shear," *J. Appl. Mech. Tech. Phys.*, **5**, 146–151 (1992).
4. K. A. Hartley, J. Duffy, and R. H. Hewley, "Measurement of the temperature profile during shear band formation in steel deformation at high strain rates," *J. Mech. Phys. Solids*, **35**, No. 3, 283–301 (1987).
5. A. Marchand and J. Duffy, "An experimental study of the formation process of adiabatic shear bands in a structural steel," *J. Mech. Phys. Solids*, **36**, No. 3, 251–283 (1987).
6. R. J. Clifton, J. Duffy, K. A. Hartley, et al., "On critical condition for shear band formation at high strain rates," *Scripta Metallurg.*, **18**, 443–448 (1984).
7. Yu. S. Zav'yalov, B. I. Kvasov, and V. L. Miroshnichenko, *Methods of Spline Functions* [in Russian], Nauka, Moscow (1980).